A fungal family of lytic polysaccharide monooxygenase-like copper proteins

Aurore Labourel, Kristian Frandsen, Feng Zhang, Nicolas Brouilly, Sacha Grisel, Mireille Haon, Luisa Ciano, David Ropartz, Mathieu Fanuel, Francis Martin, et al.

nature chemical biology

ARTICLES

https://doi.org/10.1038/s41589-019-0438-8

A fungal family of lytic polysaccharide monooxygenase-like copper proteins

Aurore Labourel[1], Kristian E. H. Frandsen[1,2], Feng Zhang[3], Nicolas Brouilly[4], Sacha Grisel[1], Mireille Haon[1], Luisa Ciano[5], David Ropartz[6], Mathieu Fanuel[6], Francis Martin[3], David Navarro[1], Marie-Noëlle Rosso[1], Tobias Tandrup[2], Bastien Bissaro[1], Katja S. Johansen[7], Anastasia Zerva[1,8], Paul H. Walton[5], Bernard Henrissat[9,10,11], Leila Lo Leggio[2] and Jean-Guy Berrin[1]*

Lytic polysaccharide monooxygenases (LPMOs) are copper-containing enzymes that play a key role in the oxidative degradation of various biopolymers such as cellulose and chitin. While hunting for new LPMOs, we identified a new family of proteins, defined here as X325, in various fungal lineages. The three-dimensional structure of X325 revealed an overall LPMO fold and a His brace with an additional Asp ligand to Cu(II). Although LPMO-type activity of X325 members was initially expected, we demonstrated that X325 members do not perform oxidative cleavage of polysaccharides, establishing that X325s are not LPMOs. Investigations of the biological role of X325 in the ectomycorrhizal fungus *Laccaria bicolor* revealed exposure of the X325 protein at the interface between fungal hyphae and tree rootlet cells. Our results provide insights into a family of copper-containing proteins, which is widespread in the fungal kingdom and is evolutionarily related to LPMOs, but has diverged to biological functions other than polysaccharide degradation.

The discovery of LPMOs has overturned much of the accepted thinking within the field of cellulose and chitin degradation[1–3]. LPMOs are copper-dependent enzymes that break down polysaccharides through an oxidative mechanism involving an electron donor and molecular oxygen or H_2O_2 (refs.[1,2,4]). LPMOs active on cellulose are able to boost the activity of cellulases to such an extent that they are now incorporated in industrial enzyme mixtures for the conversion of agricultural residues to biofuels[5]. At the active site of LPMOs, the copper ion is bound through a His brace, which comprises an N-terminal His that chelates a single copper ion through its amino terminus -NH_2 and the Nδ of its imidazole side chain. This N-terminal His residue is usually methylated by filamentous fungi[2,6] and, although recent studies have suggested a role in protecting the enzyme from self-oxidative inactivation[7], the function of this modification is yet to be fully elucidated. The copper coordination is completed by the Nε of an additional His side chain, to form an overall N_3 T-shaped geometry[8].

The recently discovered LPMO families have been identified by a 'module-walking' approach. This method relies on the fact that many carbohydrate-active enzymes (CAZymes) are multimodular with one or more additional domains, which are often substrate-targeting carbohydrate-binding modules (CBMs)[9]. The modules attached to known CAZymes were used to search for proteins, which (i) contained those modules, (ii) contained a conserved His immediately after the signal peptide cleavage site and (iii) did not display significant sequence similarity to known AA9 and AA10 families. This method has led to the discovery of several LPMO families (AA11 (ref. [10]), AA13 (refs. [11,12]) and AA15 (ref. [13])) but does not allow the identification of new LPMOs lacking additional modules. In a complementary approach that was based on comparative post-genomic analyses applied to fungal saprotrophs, we recently identified xylan-active AA14 LPMOs[14] and cellulose-active AA16 LPMOs[15]. These examples emphasized the fact that fungal secretomes are a promising ground to hunt for new LPMOs and to gain insights into their biological role[16].

Using a similar approach, here we report the discovery of a widespread copper-containing protein family, named X325, found in various fungal lineages including saprotrophic and ectomycorrhizal (ECM) fungi and yeasts. Although X325 family members share many structural features and a probable common ancestor with biomass-degrading LPMOs, their copper-binding site is atypical and more similar to those of other copper-binding proteins involved in copper homeostasis. This study reveals new prospects for LPMO-like proteins with biological functions other than polysaccharide degradation.

Results

Discovery of the X325 family. The basidiomycete *Laetisaria arvalis* (strain BRFM514) is able to grow on cellulose or wheat straw as a sole carbon source and to fully digest cellulose filter paper[17]. Global transcriptome and secretome analyses revealed that *L. arvalis* produces a unique repertoire of CAZymes, including a complete set of cellulose-acting enzymes[17]. Searching for proteins with a predicted N-terminal His among *L. arvalis* post-genomic data led to the identification of a protein of unknown function (GenBank accession MK088083, here termed 'LaX325') that was secreted

[1]INRA, Biodiversité et Biotechnologie Fongiques (BBF), UMR1163, Aix Marseille Université, Marseille, France. [2]Biological Chemistry Section, Department of Chemistry, University of Copenhagen, Copenhagen, Denmark. [3]INRA, UMR1136, Interactions Arbres/Microorganismes, Laboratoire d'Excellence ARBRE, Centre INRA-Lorraine, Université de Lorraine, Champenoux, France. [4]CNRS, IBDM, Aix Marseille Université, Marseille, France. [5]Department of Chemistry, University of York, York, UK. [6]INRA, Unité de Recherche Biopolymères Interactions Assemblages (BIA), Nantes, France. [7]Department of Geosciences and Natural Resource Management, University of Copenhagen, Copenhagen, Denmark. [8]Biotechnology Laboratory, School of Chemical Engineering, National Technical University of Athens, Zografou Campus, Athens, Greece. [9]INRA, USC1408 Architecture et Fonction des Macromolécules Biologiques (AFMB), Marseille, France. [10]Architecture et Fonction des Macromolécules Biologiques (AFMB), CNRS, Aix Marseille Université, Marseille, France. [11]Department of Biological Sciences, King Abdulaziz University, Jeddah, Saudi Arabia. *e-mail: jean-guy.berrin@inra.fr

during growth on cellulose and wheat straw. In-depth analysis of the proteomic data obtained from the *L. arvalis* secretome revealed that the N-terminal His is methylated (mass + 14.0157 Da), a feature commonly observed in fungal LPMOs[2]. Moreover, a protein-fold-recognition analysis[18] using X325 as a template matched the cellulose-active AA10 LPMO from *Streptomyces coelicolor* (PDB code 6F7E (ref. [19])) with 97% confidence but only 14% sequence identity. This level of sequence relatedness is however insufficient to group X325 with the bacterial LPMOs that mostly compose family AA10. Therefore, X325 was used as the query sequence for a BLAST search on the non-redundant protein sequence database of the NCBI database, and this retrieved approximately 550 significantly related sequences (*e* values lower than 4×10^{-4}). Alignments of the retrieved sequences (Supplementary Fig. 1) showed two conserved His residues, one being the N terminus of the mature protein, compatible with a copper-binding His brace[2], a hallmark of all known LPMOs. Interestingly, none of the X325 sequences carries a CBM but instead they invariably harbor a glycosylphosphatidylinositol (GPI) anchor at the C terminus (Supplementary Fig. 1). Usually, proteins attached to a GPI anchor via their C terminus are found in the outer leaflet of the lipid bilayer facing the extracellular environment[20]. GPI anchors can also be considered as predetermined breaking points, which allow the release of proteins into the extracellular environment upon enzymatic cleavage[20]. Release of the protein from the membrane could explain the presence of LaX325 in the secretomes of *L. arvalis*[17]. The phylogenetic analysis of X325 modules (conducted after removal of signal peptides and GPI anchors) was performed on 123 protein sequences encoded by 58 genomes selected to represent the fungal diversity (Fig. 1). The analysis showed that X325 proteins are present across the fungal kingdom including early diverging fungi within Mucoromycotina[21], saprotrophic fungi, symbiotic fungi, endophytic fungi, plant and animal pathogens, and, more surprisingly, several yeast species lacking plant-cell-wall-degrading enzymes. This was an indication that X325 proteins may have a different function than oxidative cleavage of glycoside linkages in plant biomass. The phylogenetic tree of X325 members shows that the family is divided into six distinct clades, two of which gathered basidiomycetes and the other four of which gathered ascomycetes (Fig. 1). On average 2.3 X325-encoding genes were found per fungal species.

On the basis of the X325 phylogenetic analysis, we selected several X325 candidate genes from different clades and subgroups (Fig. 1) within model fungi and yeasts, and recombinantly expressed them in *Pichia pastoris* (Supplementary Table 1). Using this method, we produced and purified four X325 proteins: LaX325 from the fungal saprotroph *L. arvalis* (GenBank accession MK088083), PaX325 from the coprophilous fungus *Podospora anserina* (GenBank accession XM_001907524.1), LbX325 from the ECM fungus *L. bicolor* (GenBank accession XM_001874260.1) and YlX325 from the yeast *Yarrowia lipolytica* (GenBank accession XM_505821.1). The correct processing of the native signal peptide, which exposed the N-terminal His residue at position 1 in the mature polypeptide chain was confirmed using N-terminal sequencing. Inductively coupled plasma mass spectrometry (ICP-MS) analyses revealed that recombinant X325 proteins contained approximately one copper atom per protein molecule.

X325 crystal structure displays a fold similar to LPMOs. The three-dimensional (3D) structure of LaX325 was solved by single-wavelength anomalous dispersion (SAD) phasing at the copper edge, and refined in three crystal forms at resolutions of around 2 Å (Supplementary Table 2). The core of the protein folds into a largely antiparallel immunoglobulin-like β-sandwich, a fold similar to that seen in LPMO structures[22] (Fig. 2a). The closest structural homolog in the PDB database according to the DALI server[23] is the recently determined *Thermobia domestica* AA15 LPMO structure

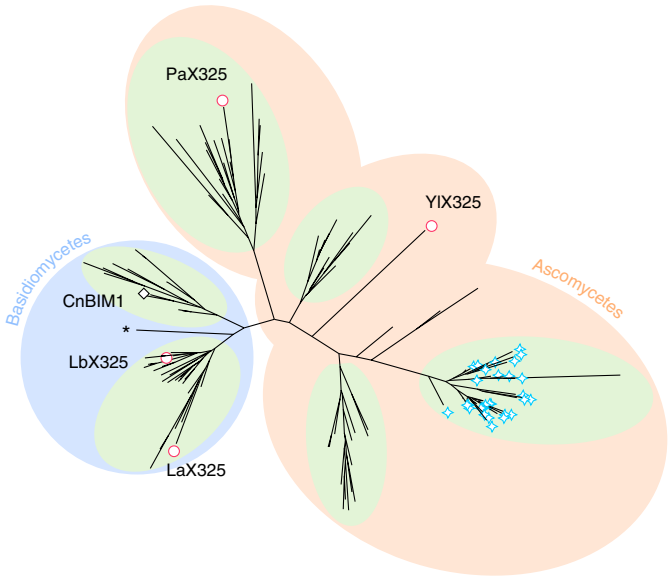

Fig. 1 | Phylogeny of the X325 family. The phylogenetic tree was built with 123 protein sequences originating from 58 different genomes. Green patches highlight the clades. Nodes with a red oval shape show the X325 proteins selected and characterized in this study. The diamond node shows the *Cryptococcus neoformans* X325 (CnBIM1). Light-blue star-shaped nodes highlight the sequences displaying a His instead of an Asp residue in the active site. The asterisk indicates the sequence belonging to early diverging Mucoromycotina (not part of basidiomycetes). Modularity and sequence alignment of the X325 family are presented in Supplementary Fig. 1.

(Supplementary Fig. 2; Protein Data Bank (PDB) accession 5MSZ; *Z* score of 11.0), closely followed by four bacterial AA10 LPMOs (PDB accessions 5FJQ, 2BEM, 5WSZ and 5L2V). Two conserved disulfides (formed by Cys22–Cys128 and Cys93–Cys145) stabilize the LaX325 structure (Supplementary Fig. 1). However, unlike LPMOs implicated in polysaccharide degradation, X325 lacks an extended binding surface capable of accommodating polysaccharide substrates. This was highlighted by comparison with LsAA9A in complex with cellohexaose (Fig. 3a). Furthermore, the GPI anchor would protrude from the face of the protein expected to bind polysaccharides (Fig. 3a) and no conservation of residues typically associated with polysaccharide binding was observed on the surface of X325 near the copper-binding site (Supplementary Fig. 3).

X325 structure reveals an unusual copper-binding site. In addition to the overall folding similarity between the structure of LaX325 and bona fide LPMOs, the canonical His brace coordination formed by two His residues (His1 and His49) is preserved and the second His is found in a loop topologically equivalent to that holding the second His in structurally characterized LPMOs, although the angle between the two imidazole planes is somewhat different than usual[8] (Fig. 2b). Tyr118 is present below the copper equatorial plane, but it is on a topologically different strand to that which is commonly found in, for example, AA9 LPMOs. Although Tyr residues within or close to axial coordination distance of the copper-binding site are a common feature in many LPMOs, in the LaX325 structures, this Tyr residue is positioned away from the metal ion (average Cu–O distance of 4.6 Å; Fig. 2b). Furthermore, this Tyr residue is not conserved across the X325 family (Supplementary Fig. 1).

In striking contrast with known LPMOs, the copper is further coordinated by an Asp side chain (Asp122; average Cu–O distance of 2.0 Å) in its flat equatorial plane. The second oxygen atom of the carboxylate of the Asp side chain lies below the flat equatorial plane of the copper at an average Cu–O distance of 2.9 Å. Above the plane,

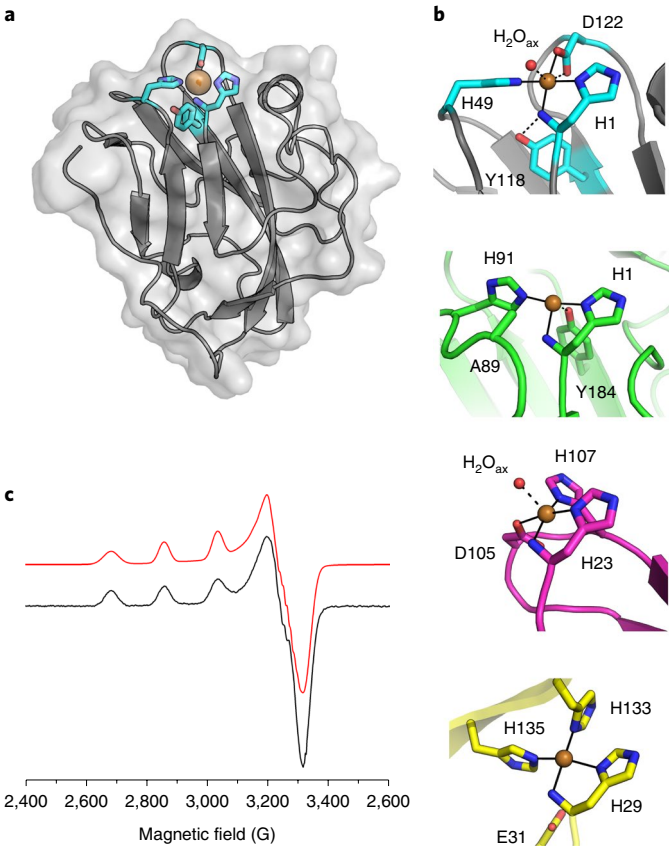

Fig. 2 | Structure of X325 and configuration of the copper active site. **a**, Overall 3D structure of LaX325 (gray) and active-site residues (cyan). **b**, Top to bottom, active sites (His brace) of LaX325 (cyan) and TdAA15 (green), and the copper-binding site of CopC (magenta) and the Cu_B center of *Methylocystis* pMMO (yellow) aligned with respect to the N-terminal His. Equatorial copper coordination is indicated with full lines. In LaX325 the copper atom is coordinated by His1, His49, Asp122 and a water molecule in the axial position (red sphere). **c**, Continuous-wave X-band EPR spectrum with simulation (red) of LaX325. More data are presented in Supplementary Figs. 2–4.

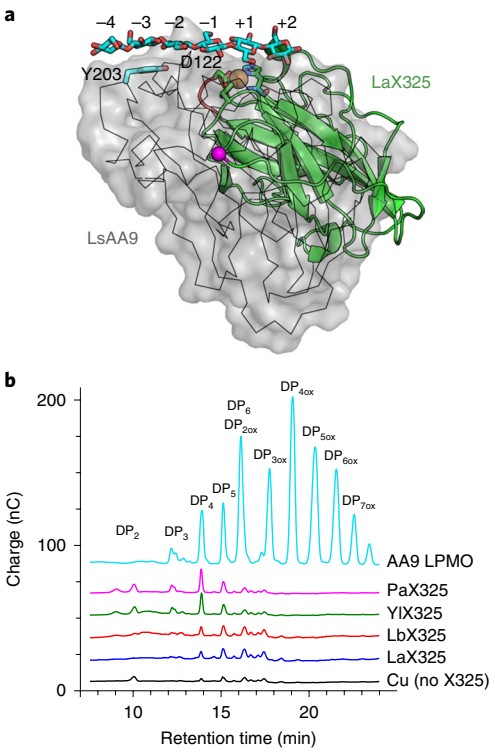

Fig. 3 | LaX325 structural and biochemical features do not support LPMO-type activity. a, Superimposition of LaX325 and LsAA9A in complex with its polysaccharide substrate (aligned with respect of the N-terminal His). The LaX325 structure (green; PDB accession 6IBJ) is shown in cartoon with His1 and Asp122 shown in sticks. The GGDG loop is shown in red and the C terminus is shown in magenta (a sphere represents the first His of the His_6 tag that substitutes the GPI anchor in the recombinant protein). The surface of LsAA9A (PDB accession 5ACI) is shown in gray and the structure is shown in ribbon (black). His1, Tyr203 and cellohexaose of LsAA9A are shown as cyan sticks. **b**, The action of X325 proteins on cellulose (Avicel) was investigated and compared to PaLPMO9E, a C1 cellulose-acting AA9 LPMO. Assays were performed in the presence of L-cysteine (1 mM). In the control condition, X325 protein was replaced by $CuSO_4$ at the same concentration (1 μM). Samples were analyzed by ionic chromatography. Cellohexaose (DP_6) is eluted at the same retention time as cellobionic acid (DP_{2ox}). The experiments were repeated three times independently. More data supporting the absence of LPMO-type activity of X325 proteins are presented in Supplementary Fig. 5.

a density identified as a fully occupied water molecule is present in the axial position of the copper-coordination sphere in both the $P2_1$ and the $P2_12_12_1$ crystal structures in four of six independent molecules. The geometry of the copper in terms of θ_1, θ_2 and θ_3 angles falls mostly within the values usually observed for Cu(II) in LPMOs[24] (Supplementary Table 3).

A similar copper coordination in the three crystal forms confirmed Asp122 as a copper ligand. Asp122 is located in a semiconserved GGDGN loop that is equivalent to loop 8 in AA9 LPMOs[22]. On the basis of its amino acid composition, the loop is likely to be flexible and perhaps move in response to a transition to Cu(I); however, no conformational change was observed in crystals treated with 5 mM L-cysteine or extensively exposed to X-rays.

Asp is not an unprecedented ligand for copper in metalloproteins. In fact, such coordination by a carboxylate is seen for LPMOs both in fusolin[25] (belonging to the AA10 family; PDB accessions 4YN2, 4OW5, 4X27 and 4X29) and NcAA9F[26] (PDB accession 4QI8) (Supplementary Table 3) crystals, but only in the crystal, as the Glu–Asp comes from a symmetry-related molecule. Additionally, the copper-binding protein CopC[27] (Fig. 2b and Supplementary Table 3) has a structurally similar binding site with a His brace and an Asp-coordinating copper, although the atomic arrangement is not identical as the Asp and one His are in swapped positions and the imidazole Nδ is coordinating the copper (rather than Nε as in canonical LPMOs). Very recently, it has been proposed that the true active site in particulate methane monooxygenase (pMMO) is found in the C subunit (Cu_C site), in which two His residues and one Asp coordinate a copper ion (PDB accessions 3RFR and 3RGB). This was previously interpreted as a zinc in a tetrahedral configuration not involving the N-terminal NH_2 of the polypeptide[28,29] and thus quite different from both LPMOs and X325. Sequence alignments of X325 members showed that the LaX325 Asp122 is mainly conserved across the family; however, in an important variation, a subgroup displays a His in this position instead (Fig. 1b and Supplementary Fig. 1). The arrangement of the copper-binding site in this subgroup could thus be very similar to that seen in the N-terminal copper-binding site (Cu_B site) of pMMOs (Fig. 2b and Supplementary Fig. 2), which was originally believed to be the active site (this, however, has now been challenged[28,30]).

X325 proteins are spectroscopically similar to LPMOs. Continuous-wave electron paramagnetic resonance (EPR) spectroscopy was

carried out on LaX325 to investigate the copper active site of this protein (Fig. 2c) for which the 3D structure was available. The spin Hamiltonian parameters determined from the simulations of the X-band spectrum (Fig. 2c and Supplementary Table 4) showed that the active site of LaX325 falls within a type 2 classification[31] ($g_z = 2.260$ and $|A_z| = 543$ MHz). Owing to the presence of the His tag, which could potentially offer a competitive binding site for the copper, a careful copper titration was performed (Supplementary Fig. 4). This titration revealed that the only observable copper species in the EPR spectra was derived from the metal bound at the His brace active site, if no excess copper was present. The spin Hamiltonian parameters, with a $d(x^2-y^2)$ semi-occupied molecular orbital (SOMO), are similar to those obtained for LPMOs, suggesting that the presence of the coordinating Asp residue does not substantially affect the coordination environment of the active site.

X325 proteins are not LPMOs. To assess whether the four different recombinantly produced X325 proteins are able to act on polysaccharide substrates in an LPMO-type manner, we performed activity assays on a wide range of plant-cell-wall polysaccharides including cellulose, xylan, xyloglucan, (1→3)-(1→4)-β-D-glucan, glucomannan, pectins and soluble oligosaccharides, as well as on fungal-cell-wall polysaccharides including chitin, chitosan, β-(1→3)-glucan, β-(1→6)-glucan, and a fungal-cell-wall extract from *L. bicolor*. No substantial level of oligomeric products was detected by ionic chromatography, except when cellulose was used as substrate, in which case, small soluble cello-oligosaccharides peaks were detected concomitantly with barely detectable peaks eluting at the same retention time as C_1-oxidized peaks. Although the oxidative nature of these C_1-oxidized peaks was confirmed by mass spectrometry (Supplementary Fig. 5), their abundance was negligible as compared to the copper control condition and to a cellulose-active AA9 LPMO[6] that produced a large amount of C_1-oxidized products (Fig. 3b). In an attempt to explore the reactivity of the X325 proteins and trigger the formation of oxidized products, other enzyme assays conditions were attempted.

Recent reports have proposed hydrogen peroxide as an alternative co-substrate[4,32,33], but addition of H_2O_2 to X325 enzyme reactions had no effect on the product released from cellulose. In the case of family AA9 LPMOs, it is well established that LPMOs can receive electrons from an external reducing agent (for example, ascorbate, cysteine or lignin) or from cellobiose dehydrogenase (CDH)[34,35]. Attempts to use either (i) lignin fractions extracted from wood, (ii) duroquinol, which is used as reducing agent for pMMOs[36], or (iii) *P. anserina* CDH under the experimental conditions used for AA9 LPMOs[22] did not trigger the formation of soluble products. Additionally, mutagenesis work in YlX325 aimed at shortening the side chain of Asp116 (equivalent to Asp122 in LaX325) to a serine residue (D116S substitution) or replacing the Asp by its pMMO analog (D116H substitution) led to the same product profile as wild-type YlX325 (that is, no activity; Supplementary Fig. 5), suggesting that the apparent lack of cellulolytic activity is not due to copper coordination by the Asp side chain. To evaluate whether X325 displayed any monooxygenase activity on cellulose, experiments were carried out in the absence of oxygen with and without addition of H_2O_2 (Supplementary Fig. 5). The release of cello-oligosaccharides was not dependent on either oxygen or H_2O_2, meaning that the presence of cello-oligosaccharides was probably due to nonspecific binding of X325 proteins to cellulose (as has already been shown for bovine serum albumin), which causes an increase in soluble reducing ends production[37].

Localization of LbX325 in *L. bicolor*. The gene encoding LbX325 is upregulated during *Laccaria–Populus* ectomycorrhizae formation and a similar trend was also observed for some X325 orthologs in some other symbiotic fungi (Supplementary Table 5). In nature, trees rely on ectomycorrhizal symbiosis to acquire the scarce nutrients available in soils[38]. It is widely accepted that ectomycorrhizal fungi have an extremely reduced enzyme portfolio to degrade plant cell walls, as their symbiotic plant partner provides them with carbon. Fungal hyphae penetrate the tree rootlets intercellularly to differentiate a hyphal network, the so-called Hartig net[39]. Although development of the Hartig net does not lead to substantial change in cell-wall composition, subtle alterations, such as localized loosening and swelling of plant cell walls accompany the hyphal ingression[40,41]. Therefore, we performed immunolabeling experiments on ECM from *L. bicolor* hyphae colonizing *Populus* roots to localize LbX325 and gain in vivo insights into its function. To do so, polyclonal antibodies were raised against purified recombinant LbX325 and their specificity was first assessed by immunoblot on *L. bicolor* ECM crude extracts (Supplementary Fig. 6). A strong signal corresponding to the molecular weight of LbX325 was detected in the fraction containing the membrane-bound proteins. This experiment supported the fungal-cell-wall localization of LbX325, which was predicted by the presence of the C-terminal GPI anchor. On ECM sections, anti-LbX325 antibodies led to an intense labeling of hyphae constituting the mantle and the Hartig net (Fig. 4). Labeling was mainly detected at the periphery of the hyphae and coincided with the location of cell-wall chitin labeled by wheat germ agglutinin (WGA), supporting a cell wall and/or apoplastic localization. In the presence of exogenous recombinant LbX325 (competitive assay), the specific binding of antibodies to X325 produced in vivo

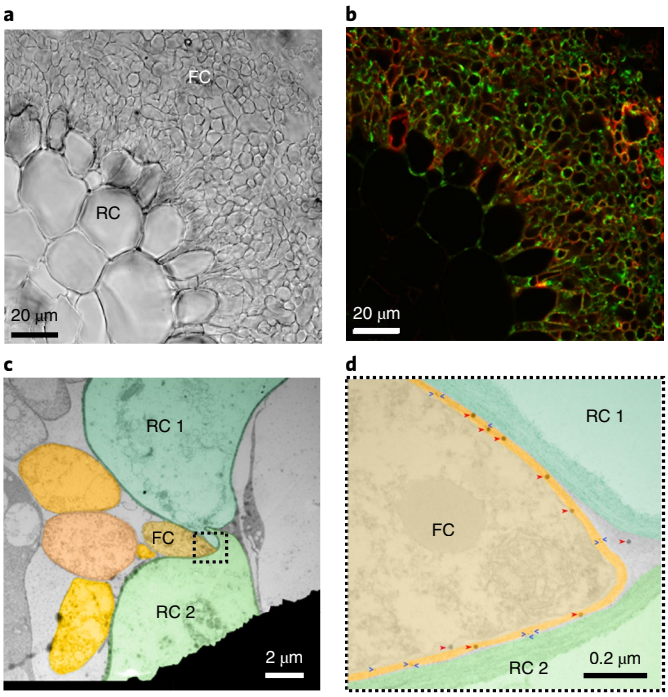

Fig. 4 | Immunolocalization of LbX325 in *L. bicolor*. **a**, Bright-field observation of transverse sections of 3-week-old ectomycorrhiza. **b**, Transverse sections of 3-week-old ectomycorrhiza stained for LbX325 with anti-LbX325 immune serum (green) and for chitin with WGA (red). Images in **a** and **b** were obtained by using indirect immunofluorescence confocal laser microscopy. **c**, Transmission electron micrograph obtained after post-embedding double-immunogold labeling of ultrathin transverse sections of 3-week-old ectomycorrhiza. **d**, Expanded view of **c**. Chitin is identified with wheat germ agglutinin (WGA) coupled to 15-nm gold particles (highlighted by red arrows). LbX325 is identified with a secondary antibody coupled to 6-nm gold particles (highlighted by blue arrows). RC, root cell, FC, fungal cell. Selected images are representative of five different sections. More data are presented in Supplementary Figs. 6–8.

by *L. bicolor* was precluded and no signal was detected, confirming the high specificity of the immune serum (Supplementary Fig. 7). No signal in the *L. bicolor* free-living mycelium (FLM) was detected using confocal miscroscopy (Supplementary Fig. 7), consistent with LbX325 transcripts being present at low level. For a better resolution, immunogold labeling was also performed on FLM and ECM, and transmission electronic microscopy confirmed the fungal-cell-wall localization of LbX325 (Fig. 4). A quantitative assessment indicated a preferential localization of LbX325 within and beyond the outer layers of the cell wall, consistent with a GPI anchor that can be cleaved off (Supplementary Fig. 8 and Supplementary Table 6). Thus, the upregulation of the gene encoding LbX325 in ECM as compared to free-living mycelium, as well as its localization, suggest the involvement of LbX325 in fungal-cell-wall remodeling during *Laccaria–Populus* symbiosis.

Discussion

The newly discovered X325 family shares several features with LPMOs, which initially led us to expect LPMO activity from proteins of this family. Indeed, they are like AA9 LPMOs in the following ways: (i) X325-encoding genes are upregulated and X325 proteins are secreted by fungi in the context of modification and degradation of plant cell walls; (ii) X325 proteins harbor two strictly conserved His residues, with one being at the N-terminal position and methylated in vivo; (iii) X325 proteins are monocopper-containing proteins with an overall structural fold similar to LPMOs; and (iv) the coordination of the copper ion by a His brace is spectroscopically similar to AA9 LPMOs and geometrically very similar to LPMOs in general. However, X325 members invariably harbor a GPI anchor at the C terminus. This feature is generally absent in fungal LPMOs. Only a subgroup of AA16 LPMO members displays this C-terminal anchor[15]. GPI-anchored proteins are often involved in biological processes such as cell-wall remodeling or transmembrane signaling[42–44]. The GPI moiety can be cleaved off by specific phospholipases, releasing the protein into the extracellular matrix and thus adding a supplemental level of regulation. Furthermore, no substantial oxidative activity could be detected on tested polysaccharides, in agreement with the analysis of the LaX325 crystal structure. Indeed, LaX325 does not display an extended flat binding surface as described in AA9 LPMOs, and no conserved aromatic residues that could promote polysaccharide binding are found in the vicinity of the copper-binding site. From a molecular point of view, the LaX325 crystal structure reveals the presence of an Asp as the third ligand in the equatorial plane of the copper-coordination sphere. As it has been proposed that LPMOs activate oxygen species at the free equatorial site, this could explain the lack of monooxygenase activity in X325 members; however, substitution of the Asp residue (equivalent to Asp122 in LaX325) did not lead to any detectable polysaccharide-degrading activity. Interestingly, some of the X325 proteins display a His in place of the LaX325 Asp122, drawing a parallel with the pMMO Cu_B site, which has been recently proposed not to be the site of oxygen activation for the oxidation of methane[28,29]. Notwithstanding the now apparent lack of oxidative activity of this site in pMMO, the single copper ion is coordinatively saturated in the equatorial coordination plane similarly to the copper site in X325. This saturation removes an obvious site for oxygen activation, thus indicating that oxidase activity does not occur either at the pMMO Cu_B site or in X325 proteins. Therefore, the role of the copper site in each of these enzymes is not clear, but the obvious parallels between the two would suggest that X325 could contribute to an overall oxidase activity in conjunction with other yet-to-be-discovered partners.

The coordination of copper in LaX325 is also similar to the Cu(II) site found in the periplasmic copper-binding protein CopC, which is believed to play a role in bacterial copper homeostasis[27]. The unusual copper-binding site, which is similar to copper-binding proteins, the absence of oxidative activity on polysaccharides and the conspicuous lack of CBMs, pose questions about the in vivo role of X325 proteins. Copper is required in multiple redox-active enzymes such as cytochrome c oxidases, multicopper oxidases or Cu–Zn superoxide dismutases and, of course, LPMOs, in which the redox cycling of the metal through its Cu(I) and Cu(II) oxidation states is an essential feature of the mechanistic chemistry, especially in reactions with oxygen and/or H_2O_2. In the same regard, an excess of copper is also implicated in the oxidation of proteins and damage to membrane lipids and DNA. Indeed, the uncontrolled activation of oxygen or H_2O_2 by reduced transition metals leads to harmful reactive oxygen species. This dual effect forces organisms to maintain a precise copper homeostasis to enable protein function whilst avoiding metal toxicity[45,46]. From this point of view, in ECM fungi, metal transporters, especially those related to copper trafficking, display the highest expression levels in mycorrhizae, suggesting extensive translocation of copper to plant root cells and possibly to fungal metalloenzymes that are strongly upregulated in symbiotic hyphae[47]. Indeed, upregulation of the gene encoding LbX325 was observed during *Laccaria–Populus* ectomycorrhizal formation and also during fruiting body formation. These data draw a parallel with other work[48] showing that the knockout mutation of one of the genes encoding *P. anserina* X325 (GenBank accession XP_001907047.1, termed *IDC2*) led to an "impaired for the development of crippled growth" phenotype, an epigenetic cell degeneration associated with slow and abnormal growth, as well as with sterility. In the endophytic fungus *Epichloë festucae*, the X325-encoding gene *SymB* (GenBank accession KX827271.1; sharing 75% identity with *IDC2*) is required for hyphal cell–cell fusion and maintenance of a mutualistic interaction with ray grass (*Lolium perenne*)[49]. The X325 family also includes Bim1 from the pathogenic fungus *Cryptococcus neoformans*, in which it is a critical factor in copper acquisition in fungal meningitis[50]. Altogether, these data suggest that, in vivo, X325 proteins may have an important role related to the morphogenesis and development of the fungus, as well as symbiosis with plants (in fungi for which this is a relevant part of the life cycle).

Therefore, CnBIM1, IDC2, SymB and the other members of the X325 family studied here seem to hold biological functions in which copper is central. To understand the biological role of X325 proteins in filamentous fungi of different lifestyles, the interplay between X325 proteins and copper must be further investigated.

Online content

Any methods, additional references, Nature Research reporting summaries, source data, extended data, supplementary information, acknowledgements, peer review information; details of author contributions and competing interests; and statements of data and code availability are available at https://doi.org/10.1038/s41589-019-0438-8.

Received: 9 January 2019; Accepted: 22 November 2019;
Published online: 13 January 2020

References

1. Vaaje-Kolstad, G. et al. An oxidative enzyme boosting the enzymatic conversion of recalcitrant polysaccharides. *Science* **330**, 219–222 (2010).
2. Quinlan, R. J. et al. Insights into the oxidative degradation of cellulose by a copper metalloenzyme that exploits biomass components. *Proc. Natl Acad. Sci. USA* **108**, 15079–15084 (2011).
3. Horn, S. J., Vaaje-Kolstad, G., Westereng, B. & Eijsink, V. G. Novel enzymes for the degradation of cellulose. *Biotechnol. Biofuels* **5**, 45 (2012).
4. Bissaro, B. et al. Oxidative cleavage of polysaccharides by monocopper enzymes depends on H_2O_2. *Nat. Chem. Biol.* **13**, 1123 (2017).
5. Johansen, K. S. Discovery and industrial applications of lytic polysaccharide mono-oxygenases. *Biochem. Soc. Trans.* **44**, 143–149 (2016).
6. Bennati-Granier, C. et al. Substrate specificity and regioselectivity of fungal AA9 lytic polysaccharide monooxygenases secreted by *Podospora anserina*. *Biotechnol. Biofuels* **8**, 90 (2015).

7. Petrović, D. M. et al. Methylation of the N-terminal histidine protects a lytic polysaccharide monooxygenase from auto-oxidative inactivation. *Protein Sci.* **27**, 1636–1650 (2018).
8. Ciano, L., Davies, G. J., Tolman, W. B. & Walton, P. H. Bracing copper for the catalytic oxidation of C–H bonds. *Nat. Catal.* **1**, 571–577 (2018).
9. Gilbert, H. J., Knox, J. P. & Boraston, A. B. Advances in understanding the molecular basis of plant cell wall polysaccharide recognition by carbohydrate-binding modules. *Curr. Opin. Struc. Biol.* **23**, 669–677 (2013).
10. Hemsworth, G. R., Henrissat, B., Davies, G. J. & Walton, P. H. Discovery and characterization of a new family of lytic polysaccharide monooxygenases. *Nat. Chem. Biol.* **10**, 122–126 (2014).
11. Lo Leggio, L. et al. Structure and boosting activity of a starch-degrading lytic polysaccharide monooxygenase. *Nat. Commun.* **6**, 5961 (2015).
12. Vu, V. V., Beeson, W. T., Span, E. A., Farquhar, E. R. & Marletta, M. A. A family of starch-active polysaccharide monooxygenases. *Proc. Natl Acad. Sci. USA* **111**, 13822–13827 (2014).
13. Sabbadin, F. et al. An ancient family of lytic polysaccharide monooxygenases with roles in arthropod development and biomass digestion. *Nat. Commun.* **9**, 756 (2018).
14. Couturier, M. et al. Lytic xylan oxidases from wood-decay fungi unlock biomass degradation. *Nat. Chem. Biol.* **14**, 306 (2018).
15. Filiatrault-Chastel, C. et al. AA16, a new lytic polysaccharide monooxygenase family identified in fungal secretomes. *Biotech. Biofuels* **12**, 55 (2019).
16. Berrin, J.-G., Rosso, M.-N. & Abou Hachem, M. Fungal secretomics to probe the biological functions of lytic polysaccharide monooxygenases. *Carbohydr. Res.* **448**, 155–160 (2017).
17. Navarro, D. et al. Fast solubilization of recalcitrant cellulosic biomass by the basidiomycete fungus *Laetisaria arvalis* involves successive secretion of oxidative and hydrolytic enzymes. *Biotechnol. Biofuels* **7**, 143 (2014).
18. Kelley, L. A., Mezulis, S., Yates, C. M., Wass, M. N. & Sternberg, M. J. E. The Phyre2 web portal for protein modeling, prediction and analysis. *Nat. Protoc.* **10**, 845–858 (2015).
19. Forsberg, Z. et al. Structural and functional characterization of a conserved pair of bacterial cellulose-oxidizing lytic polysaccharide monooxygenases. *Proc. Natl Acad. Sci. USA* **111**, 8446–8451 (2014).
20. Low, M. & Saltiel, A. Structural and functional roles of glycosyl-phosphatidylinositol in membranes. *Science* **239**, 268–275 (1988).
21. Berbee, M. L., James, T. Y. & Strullu-Derrien, C. Early diverging fungi: diversity and impact at the dawn of terrestrial life. *Annu. Rev. Microbiol.* **71**, 41–60 (2017).
22. Tandrup, T., Frandsen, K. E. H., Johansen, K. S., Berrin, J.-G. & Lo Leggio, L. Recent insights into lytic polysaccharide monooxygenases (LPMOs). *Biochem. Soc. Trans.* **46**, 1431–1447 (2018).
23. Holm, L. & Laakso, L. M. Dali server update. *Nucleic Acids Res.* **44**, W351–W355 (2016).
24. Vu, V. V. & Ngo, S. T. Copper active site in polysaccharide monooxygenases. *Coord. Chem. Rev.* **368**, 134–157 (2018).
25. Chiu, E. et al. Structural basis for the enhancement of virulence by viral spindles and their in vivo crystallization. *Proc. Natl Acad. Sci. USA* **112**, 3973–3978 (2015).
26. Tan, T.-C. et al. Structural basis for cellobiose dehydrogenase action during oxidative cellulose degradation. *Nat. Commun.* **6**, 7542 (2015).
27. Lawton, T. J., Kenney, G. E., Hurley, J. D. & Rosenzweig, A. C. The CopC family: structural and bioinformatic insights into a diverse group of periplasmic copper binding proteins. *Biochemistry* **55**, 2278–2290 (2016).
28. Ross, M. O. et al. Particulate methane monooxygenase contains only mononuclear copper centers. *Science* **364**, 566–570 (2019).
29. Liew, E. F., Tong, D., Coleman, N. V. & Holmes, A. J. Mutagenesis of the hydrocarbon monooxygenase indicates a metal centre in subunit-C, and not subunit-B, is essential for copper-containing membrane monooxygenase activity. *Microbiology* **160**, 1267–1277 (2014).
30. Cao, L., Caldararu, O., Rosenzweig, A. C. & Ryde, U. Quantum refinement does not support dinuclear copper sites in crystal structures of particulate methane monooxygenase. *Angew. Chem. Int. Ed. Eng.* **57**, 162–166 (2018).
31. Peisach, J. & Blumberg, W. E. Structural implications derived from the analysis of electron paramagnetic resonance spectra of natural and artificial copper proteins. *Arch. Biochem. Biophys.* **165**, 691–708 (1974).
32. Kuusk, S. et al. Kinetics of H_2O_2-driven degradation of chitin by a bacterial lytic polysaccharide monooxygenase. *J. Biol. Chem.* **293**, 523–531 (2018).
33. Hangasky, J. A., Iavarone, A. T. & Marletta, M. A. Reactivity of O_2 versus H_2O_2 with polysaccharide monooxygenases. *Proc. Natl Acad. Sci. USA* **115**, 4915–4920 (2018).
34. Phillips, C. M., Beeson, W. T., Cate, J. H. & Marletta, M. A. Cellobiose dehydrogenase and a copper-dependent polysaccharide monooxygenase potentiate cellulose degradation by *Neurospora crassa*. *ACS Chem. Biol.* **6**, 1399–1406 (2011).
35. Bey, M. et al. Cello-oligosaccharide oxidation reveals differences between two lytic polysaccharide monooxygenases (family GH61) from *Podospora anserina*. *Appl. Environ. Microbiol.* **79**, 488–496 (2013).
36. Chen, K. H. et al. Bacteriohemerythrin bolsters the activity of the particulate methane monooxygenase (pMMO) in *Methylococcus capsulatus* (Bath). *J. Inorg. Biochem.* **111**, 10–17 (2012).
37. Bernardes et al. Carbohydrate binding modules enhance cellulose enzymatic hydrolysis by increasing access of cellulases to the substrate. *Carbohydr. Polym.* **211**, 57–68 (2019).
38. Shah, F. et al. Ectomycorrhizal fungi decompose soil organic matter using oxidative mechanisms adapted from saprotrophic ancestors. *New Phytol.* **209**, 1705–1719 (2016).
39. Balestrini R. M. & Kottke I. In *Molecular Mycorrhizal Symbiosis* (ed. Martin, F.) 47–62 (John Wiley & Sons, 2016).
40. Balestrini, R., Hahn, M. G., Faccio, A., Mendgen, K. & Bonfante, P. Differential localization of carbohydrate epitopes in plant cell walls in the presence and absence of arbuscular mycorrhizal fungi. *Plant Physiol.* **111**, 203–213 (1996).
41. Balestrini, R. & Bonfante, P. Cell wall remodeling in mycorrhizal symbiosis: a way towards biotrophism. *Front. Plant Sci.* **5**, 237 (2014).
42. Yamazaki, H., Tanaka, A., Kaneko, J.-i, Ohta, A. & Horiuchi, H. *Aspergillus nidulans* ChiA is a glycosylphosphatidylinositol (GPI)-anchored chitinase specifically localized at polarized growth sites. *Fungal Genet. Biol.* **45**, 963–972 (2008).
43. Nakajima, M., Yamashita, T., Takahashi, M., Nakano, Y. & Takeda, T. A novel glycosylphosphatidylinositol-anchored glycoside hydrolase from *Ustilago esculenta* functions in β-1,3-glucan degradation. *Appl. Environ. Microbiol.* **78**, 5682–5689 (2012).
44. Smith, H. W. & Marshall, C. J. Regulation of cell signalling by uPAR. *Nat. Rev. Mol. Cell Biol.* **11**, 23–36 (2010).
45. Gaggelli, E., Kozlowski, H., Valensin, D. & Valensin, G. Copper homeostasis and neurodegenerative disorders (Alzheimer's, prion, and Parkinson's diseases and amyotrophic lateral sclerosis). *Chem. Rev.* **106**, 1995–2044 (2006).
46. García-Santamarina, S. & Thiele, D. J. Copper at the fungal pathogen–host axis. *J. Biol. Chem.* **290**, 18945–18953 (2015).
47. Bolchi, A. et al. Genome-wide inventory of metal homeostasis-related gene products including a functional phytochelatin synthase in the hypogeous mycorrhizal fungus *Tuber melanosporum*. *Fungal Genet. Biol.* **48**, 573–584 (2011).
48. Lalucque, H. et al. IDC2 and IDC3, two genes involved in cell non-autonomous signaling of fruiting body development in the model fungus *Podospora anserina*. *Dev. Biol.* **421**, 126–138 (2017).
49. Green, K. A. et al. SymB and SymC, two membrane associated proteins, are required for *Epichloë festucae* hyphal cell–cell fusion and maintenance of a mutualistic interaction with *Lolium perenne*. *Mol. Microbiol.* **103**, 657–677 (2016).
50. García-Santamarina, S. et al. A lytic polysaccharide monooxygenase-like protein functions in copper import and fungal meningitis. *Nat. Chem. Biol.* https://doi.org/10.1038/s41589-019-0437-9.

Methods

Transcriptomics and secretomics data. Transcriptomic and proteomic data of cultures of *L. arvalis* strain BRFM514 grown on cellulose (Avicel), wheat straw and wheat-straw residue following traditional saccharification and maize bran are described in ref. [17]. Transcriptomic data of *L. bicolor* strain S238N are described in ref. [51].

Bioinformatic analysis of X325. *L. arvalis* X325 sequence (Genbank accession MK088083) was compared to the NCBI non-redundant sequence database using BlastP[52] in December 2017. Blast searches conducted with X325 did not retrieve AA9s, AA10s, AA11s, AA13s, AA14s or AA15s with significant scores. MUSCLE[53] was used to perform multiple alignments. To avoid interference from the presence or absence of additional residues, the signal peptides and C-terminal extensions (linker and GPI anchor) were removed. Bioinformatic analyses were performed on 58 fungal genomes sequenced and shared by JGI collaborators. A phylogenetic tree has been inferred using 123 cleaned and merged alignments of proteins from selected clusters of proteins. Those clusters are present, as much as possible, in all fungi in one copy to maximize the score $\sum 1/n$, where n is the number of copies in the genome). Sequences from clusters were aligned with MUSCLE and a phylogenetic tree was built using BOOSTER[54] (https://booster.pasteur.fr/) with a workflow involving 200 Bootstrap replicates and Fasttree. The tree is displayed with Dendroscope[55].

Production of X325 proteins. The sequences encoding LaX325 (Genbank accession MK088083), LbX325 (Genbank accession XM_001874260.1), PaX325 (Genbank accession XM_001907524.1) and YlX325 (Genbank ID XM_505821.1) genes were synthesized after codon optimization for expression in *P. pastoris* (GenScript). The region corresponding to the native signal sequence was kept and the C-terminal GPI anchor was removed. Synthesized genes were further inserted into a modified pPICZαA vector (Invitrogen) using BstBI and XbaI restriction sites in frame with the His_6 tag located at the C terminus of recombinant proteins. Site-directed mutagenesis of the Asp116 residue of YlX325 to either a Ser or His residue was performed using the Quikchange site-directed mutagenesis kit (Agilent) following manufacturer's conditions. Transformation of competent *P. pastoris* X33 was performed by electroporation with PmeI-linearized pPICZαA recombinant plasmids and zeocin-resistant *P. pastoris* transformants were screened for protein production as described[56]. The best-producing transformants were grown in 2 l of BMGY medium in shaken flasks at 30 °C in an orbital shaker (200 rpm) to an optical density at 600 nm of between 2 and 6. Cells were then transferred to 400 ml of BMMY medium containing 1 ml l^{-1} of PTM_4 salts at 20 °C in an orbital shaker (200 rpm) for 3 d, with supplementation of 3% (vol/vol) methanol every day. *P. pastoris* strain X33 and the pPICZαA vector are components of the *P. pastoris* Easy Select Expression System (Invitrogen). All media and protocols are described in the manufacturer's manual (Invitrogen).

Purification of X325 proteins. The culture supernatants were recovered by pelleting the cells by centrifugation at 2,700*g* for 5 min at 4 °C and filtering on 0.45-µm filters (Millipore). For His_6-tagged enzymes, the pH was adjusted to 7.8 and the supernatants were loaded onto 5-ml His Trap HP columns (GE Healthcare) connected to an Akta Xpress system (GE healthcare). Before loading, the columns were equilibrated in 50 mM Tris HCl, pH 7.8, 150 mM NaCl (buffer A). The loaded columns were then washed with five column volumes of 10 mM imidazole in buffer A, before the elution step with five column volumes of 150 mM imidazole in buffer A. Fractions containing the protein were pooled and concentrated with a 3-kDa vivaspin concentrator (Sartorius) and buffer exchanged in 50 mM sodium acetate buffer, pH 5.2. The concentrated proteins were then incubated with a tenfold molar equivalent of $CuSO_4$ overnight in a cold room and buffer exchanged in 50 mM sodium acetate buffer, pH 5.2 to remove $CuSO_4$ excess.

Biochemical analysis of X325 proteins. Concentration of purified proteins was determined by using a NanoDrop ND-2000 device with calculated molecular mass and molar extinction coefficients derived from the sequences. Proteins were loaded onto 10% SDS-PAGE gels (Thermo Fisher Scientific), which were stained with Coomassie Blue. The molecular mass under denaturating conditions was determined with reference standard proteins (Page Ruler Prestained Protein Ladder, Thermo Fisher Scientific).

Determination of N-terminal amino acid sequences. The N-terminal amino acid sequence of purified LaX325 was determined according to the Edman degradation. Samples were electroblotted onto a polyvinylidene difluoride membrane (iBlot, Life Technologies). Analyses were carried out on a Procise Sequencing System (Thermo Fisher Scientific).

Tandem mass spectrometry analyses. Experiments were performed on a Synapt G2Si high-definition mass spectrometer (Waters) equipped with an electrospray ion source. Oxidized species were isolated and fragmented by collision-induced dissociation in the transfer cell of the instrument (tandem mass spectrometer). In these experiments, ion mobility was activated to reduce interference from sample impurities. Ion mobility was performed in a traveling-wave ion mobility cell. Helium flow was held at 180 ml min^{-1} in the helium cell and nitrogen flow was adjusted at 90 ml min^{-1} in the mobility cell. The IM traveling-wave height was set to 40 V, and its wave velocity was set to 300 m s^{-1}. Samples were diluted tenfold in methanol–H_2O (1:1, vol/vol) and infused at a flow rate of 5 µl min^{-1}. Acquisitions were conducted in negative polarity, as well as in 'sensitivity' mode.

Inductively coupled plasma mass spectrometry analysis. Before the analysis, samples were mineralized in a mixture containing two parts HNO_3 (Sigma-Aldrich, 65% Purissime) and one part HCl (Fluka, 37%, Trace Select) at 120 °C. The residues were diluted in ultrapure water (2 ml) before ICP-MS analysis. The ICP-MS instrument was an ICAP Q (ThermoElectron), equipped with a collision cell. The calibration curve was obtained by dilution of a certified multielement solution (Sigma-Aldrich). Copper concentrations were determined using Plasmalab software (ThermoElectron), at a mass of interest (m/z) of 63.

Polysaccharide cleavage assays. Avicel was purchased from Sigma-Aldrich and lichenan (from Icelandic moss), xylan, tamarind xyloglucan, barley β-1,3/1,4-glucan, konjac glucomannan, wheat arabinoxylan, pachyman, pustulan, chitin and chitosan were purchased from Megazyme. The *L. bicolor* cell-wall extract was provided by F. Zhang (INRA).

All the cleavage assays contained 1 µM enzyme or 1 µM $CuSO_4$ in the presence of 1 mM L-cysteine, 0.5% (wt/vol) polysaccharides and 50 mM sodium acetate bufferm, pH 5.2. Lignin fractions extracted from softwood and duroquinol (Sigma-Aldrich) were also tested as reducing agents. The enzyme reactions were performed in 2-ml tubes and incubated in a thermomixer (Eppendorf) at 40 °C and 850 rpm. After 16 h of incubation, samples were heated for 10 min at 100 °C to stop the enzymatic reaction and then centrifuged at 14,000*g* for 15 min at 4 °C to separate the soluble fraction from the remaining insoluble fraction before determination of soluble products using high-performance anion-exchange chromatography as described above with oligosaccharide standards (Megazyme).

Polysaccharide cleavage assays under anaerobic conditions. To assess the monooxygenase activity of X325 proteins, the different reagent solutions used to compose the reaction mixtures were made anaerobic separately. Solutions of water, buffer (200 mM sodium acetate, pH 5.2), Avicel (1% (wt/vol)) and NaOH (2 M) were submitted to 10 min of sonication followed by 10 min of flushing with nitrogen gas before being placed in an anaerobic chamber (Jacomex GP Campus) for 48 h to ensure complete oxygen-free conditions (the lids of the vessels were slightly loose). The stock solution of copper-loaded protein and $CuSO_4$ were frozen in liquid nitrogen and allowed to thaw in the anaerobic chamber to equilibrate with the anaerobic atmosphere over 48 h. L-Cysteine was placed in the anaerobic chamber as a powder during 48 h and dissolved in anaerobic water before the experiment.

To set up reactions, the copper-loaded protein or $CuSO_4$ (5 µM final concentration) was added to anaerobic Avicel suspension (0.5% (wt/vol) final concentration) in 50 mM sodium acetate buffer, pH 5.2. L-Cysteine was added to all the reactions to a final concentration of 1 mM. H_2O_2 (50 µm) was added to the first part of the reactions, whereas water was added to the second and third parts of the reactions to a final volume of 200 µl. While the second part was kept in the anaerobic chamber (that is, under anaerobic control), the third part was taken out of the anaerobic chamber and re-equilibrated with atmospheric oxygen by vigorous mixing. The aerobic reactions constitute positive controls ensuring that the treatment of the different stock solutions (enzyme, L-cysteine) did not harm the integrity of the reactants. After 16 h of incubation at 23 °C, all reactions were stopped by addition of 10 µl of NaOH solution (0.1 M final concentration). All samples were centrifuged before analysis of soluble products by high-performance anion-exchange chromatography with pulsed amperometric detection as described above. Reactions were performed as triplicate independent experiments.

Production of antibodies, protein electrophoresis and immunoblotting. A solution of 5 mg of purified recombinant LbX325 protein was used to elicit rabbit polyclonal antibodies according to the manufacturer's procedure (Eurogentec). Total proteins from free-living mycelium and 15 ectomycorrhizal roots were extracted according to the literature[57]. Protein analyses were carried out by using 4–20% Mini-Protean TGX precast protein gels in a Mini-Protean electrophoresis cell system (both Bio-Rad). Specificity of the antibodies was determined by immunoblot of total protein obtained from poplar lateral roots not in contact with *L. bicolor* S238N and from mycorrhizal root tips using the Bio-Rad alkaline phosphatase immunoblot kit (Bio-Rad Laboratories) according to the manufacturer's instructions.

Confocal microscopy and indirect immunofluorescence localization. Three-week-old ectomycorrhizal root tips from gray poplar (cv INRA 717-1-B4) or free-living mycelium of *L. bicolor* S238N were fixed for 4 h in 4% (wt/vol) paraformaldehyde in PBS (137 mM NaCl, 2.7 mM KCl, 10 mM Na_2HPO_4, 1.8 mM K_2HPO_4, pH 7.4). The root segments were embedded in agarose 4% (wt/vol) and cut into 25-µm longitudinal or 25- to 30-µm radial sections with a Leica VT1200S Leica vibratome (Leica Microsystems). Sections were retrieved with a brush and carefully transferred onto watch glasses and then stained according to the

literature[58]. The indirect immunofluorescent localization of the LbX325 protein was performed by confocal microscopy as described[59].

Transmission electron microscopy. Three-week-old ectomycorrhizal root tips from gray poplar (cv INRA 717-1-B4) or free-living mycelium (FLM) of *L. bicolor* S238N were dissected from the agar plate and fixed with 2.5% glutaraldehyde and 2% paraformaldehyde in PBS for 2 h. The samples were washed in PBS and embedded in 4% agarose. Vibratome sections of 80 µm in thickness were made and post-fixed in 1% osmium tetroxide in distilled water for 1 h, washed and incubated in uranyl acetate (1%) in distilled water overnight at 4 °C. Vibratome sections were dehydrated in ethanol and acetone, and embedded in epon resin. Ultrathin 70-nm-thick sections were performed on a UC7 Leica Ultramicrotome (Leica).

Sections on nickel grids were incubated with saturated sodium metaperiodate for 2 min. The grids were washed rapidly in TBS with 1% Triton X-100. The grids were then incubated with 10% normal serum in TBS for 1 h, followed by an overnight incubation with rabbit anti-LbX325 antibodies (1/20) at 4 °C. The grids were washed in TBS and incubated with secondary antibodies (6-nm anti-rabbit, Aurion, 1/15) for 1 h, then washed again in TBS. The grids were incubated for 10 min in 2.5% glutaraldehyde in 0.05 M cacodylate buffer, washed and free aldehydes groups were quenched (0.1 M glycine in TBS for 10 min). The grids were then stained with WGA–15-nm conjugate for 40 min, washed in water and counterstained by 1% uranyl acetate (5 min) and lead citrate (2 min). Acquisitions were performed on a Tecnai G2 at 200 kV (FEI). Micrographs were acquired with a Veleta camera (Olympus).

Structure determination by X-ray crystallography. To remove *N*-linked glycans, 20 mg of purified enzymes were treated with 500,000 U of EndoH (New England Biolabs) under native conditions (48 h at 20 °C) according to the manufacturer's instructions. Deglycosylated and control samples were analyzed by SDS-PAGE (Supplementary Fig. 9). To remove EndoH, buffer A was added to the sample and purification was performed using a 5-ml His Trap HP columns (GE Healthcare) connected to an Akta Xpress system (GE Healthcare) as described above. Fractions containing the protein were pooled and concentrated with a 3-kDa vivaspin concentrator (Sartorius) and buffer exchanged in 20 mM MES buffer, pH 6.0.

Crystals were grown using the sitting-drop vapor diffusion technique set up in MRC plates (Molecular Dimensions) with 100-µl reservoirs at room temperature, using an Oryx-8 robot (Douglas Instruments). LaX325 (13.3 mg ml^{-1} in 20 mM MES, pH 6.0) was incubated with copper acetate in a 1:1 molar ratio for 1 h at 4 °C. Addition of copper acetate made the sample precipitate; however, the precipitate dissolved again after 1 h incubation. Screening was carried out using the commercial JCSG+ and Morpheus screens (Molecular Dimensions). Crystals were harvested and flash frozen in liquid nitrogen without added cryoprotectant. Two initial datasets were collected at a wavelength of 0.9799 Å at the BioMAX beamline of MAX-IV on LaX325 crystals grown from Morpheus conditions #40 ($P2_1$ dataset; in Supplementary Table 2) and #85 ($P4_32_12$ dataset; Supplementary Table 2) in a volume ratio of 1:1 (enzyme:reservoir solution) and 13.3 mg ml^{-1} LaX325 in the protein stock solution. Morpheus screen #40 has the following composition: 20 mM 1,6-hexanediol, 20 mM 1-butanol, 20 mM (*RS*)1,2-propandiol, 20 mM 2-propanol, 20 mM 1,4-butandiol, 2 mM 1,3-propandiol, 100 mM MES monohydrate, pH 6.5, 100 mM imidazole, pH 6.5, 12.5% (wt/vol) MPD, 12.5% (wt/vol) PEG 1,000 and 12.5% (wt/vol) PEG 3,350. Morpheus screen #85 has the following composition: 20 mM L-Na-glutamate, 20 mM DL-alanine (racemic), 20 mM glycine, 20 mM DL-lysine HCl (racemic), 20 mM DL-serine (racemic), 100 mM MES monohydrate, pH 6.5, 100 mM imidazole, pH 6.5, 20% (wt/vol) PEG 500 MME and 10% (wt/vol) PEG 20,000. The structure could not be determined from these datasets owing to limited anomalous signal at the data collection wavelength. The original crystals could not be reproduced spontaneously, but required seeding, either using the Oryx-8 robot, or by streak seeding using a horse hair. A third dataset ($P2_12_12_1$ dataset; Supplementary Table 2) was collected from a crystal of LaX325 grown by streak seeding into the Morpheus[60] #85 condition. Data was collected at beamline ID29 at the ESRF, using a wavelength of 1.299 Å, close to the copper edge, with an oscillation of 0.1° and 4,000 images for high redundancy. The structure was solved using anomalous dispersion methods, by running Phenix.autosol[61] searching for four to six sites (as indicated by the Matthew's coefficient) using data automatically processed and scaled to a resolution of 2.08 Å in $P2_12_12_1$ with XDS and XSCALE[62]. Two additional structures in different space groups were determined by molecular replacement with MOLREP[63] and refined with Refmac5 (ref. [64]) (of the CCP4 suite) using this initial structure (in $P2_12_12_1$) as search model and the previously collected $P4_32_12$ and $P2_1$ datasets scaled to resolutions of 2.10 Å and 1.82 Å, respectively. For all structures, 100% of the residues were in the allowed regions of the Ramachandran plot. Crystals of LaX325 grown from seeds in Morpheus conditions #40 and #85 were soaked for 50–60 min in 5 mM L-cysteine (Sigma-Aldrich) dissolved in reservoir conditions. Diffraction data could be collected to close to a resolution of 2 Å at the P11 beamline of Petra-III, DESY, Hamburg, Germany, but only on orthorhombic crystals. No dataset collected resulted in any conformational changes of amino acids as a function of the reduction of the copper atom. The maximum dose experienced by the crystals was estimated to 724.78 KGy using RADDOSE-3D[65]. All datasets were collected at cryogenic temperatures (100 K). Crystallization attempts of LbX325 were not successful.

Electron paramagnetic resonance spectroscopy. Continuous-wave X-band frozen solution EPR spectra of a 0.2 mM solution of Cu(II)–LaX325 in 50 mM sodium acetate buffer, pH 5.2 were recorded on a Bruker EMX spectrometer operating at ~9.30 GHz, with modulation amplitude of 4 G, modulation frequency of 100 kHz and microwave power of 10.02 mW at 165 K. To check possible binding of copper to the His tag, a copper titration was performed starting from the apo-enzyme and adding 0.2 equivalents of copper (from a $CuCl_2$ stock in water) in 2-µl injections, which showed binding exclusively to the LPMO active site until addition of approximately one equivalent of copper (Supplementary Fig. 3). Addition of Avicel to the EPR sample did not cause any change to the spectrum of LaX325.

Spectral simulations were carried out using EasySpin 5.2.16 integrated in MatLab software. Simulation parameters are given in Supplementary Table 4. It was assumed that g and A tensors were axially coincident. g_z and $|A_z|$ values were determined accurately from the absorption at low field. Accurate determination of the g_x, g_y, $|A_x|$ and $|A_y|$ values was not possible owing to the second-order nature of the perpendicular region, although it was noted that satisfactory simulation could only be achieved with the particular set of values reported in Supplementary Table 4. Furthermore, it was noted that the simulations were improved by the addition of coupled nitrogen atoms, although the exact value of the coupling could not be determined given the lack of well resolved superhyperfine coupling. Raw EPR data are available on request through Research Data York (https://doi.org/10.15124/a034974e-2782-415e-8b02-2b6e4098760e).

Reporting Summary. Further information on research design is available in the Nature Research Reporting Summary linked to this article.

Data availability

LaX325 nucleotide sequence was deposited in GenBank under accession number MK088083. The X-ray structures of LaX325 were deposited in the Protein Data Bank under accession numbers 6IBH, 6IBI and 6IBJ. Raw EPR data are available on request through the Research Data York (https://doi.org/10.15124/a034974e-2782-415e-8b02-2b6e4098760e).

References

51. Kohler, A. et al. Convergent losses of decay mechanisms and rapid turnover of symbiosis genes in mycorrhizal mutualists. *Nat. Genet.* **47**, 410–415 (2015).
52. Altschul, S. F., Gish, W., Miller, W., Myers, E. W. & Lipman, D. J. Basic local alignment search tool. *J. Mol. Biol.* **215**, 403–410 (1990).
53. Edgar, R. C. MUSCLE: multiple sequence alignment with high accuracy and high throughput. *Nucleic Acids Res.* **32**, 1792–1797 (2004).
54. Lemoine, F. et al. Renewing Felsenstein's phylogenetic bootstrap in the era of big data. *Nature* **556**, 452–456 (2018).
55. Huson, D. H. & Scornavacca, C. Dendroscope 3: an interactive tool for rooted phylogenetic trees and networks. *Syst. Biol.* **61**, 1061–1067 (2012).
56. Haon, M. et al. Recombinant protein production facility for fungal biomass-degrading enzymes using the yeast *Pichia pastoris*. *Front. Microbiol.* **6**, 1002 (2015).
57. Pitarch, A., Sánchez, M., Nombela, C. & Gil, C. Sequential fractionation and two-dimensional gel analysis unravels the complexity of the dimorphic fungus *Candida albicans* cell wall proteome. *Mol. Cell. Proteom.* **1**, 967–982 (2002).
58. Felten, J. et al. The ectomycorrhizal fungus *Laccaria bicolor* stimulates lateral root formation in poplar and *Arabidopsis* through auxin transport and signaling. *Plant Physiol.* **151**, 1991–2005 (2009).
59. Martin, F. et al. The genome of *Laccaria bicolor* provides insights into mycorrhizal symbiosis. *Nature* **452**, 88–92 (2008).
60. Gorrec, F. The MORPHEUS protein crystallization screen. *J. Appl. Crystallogr.* **42**, 1035–1042 (2009).
61. Terwilliger, T. C. et al. Decision-making in structure solution using Bayesian estimates of map quality: the PHENIX AutoSol wizard. *Acta Cryst. D Biol. Crystallogr.* **65**, 582–601 (2009).
62. Kabsch, W. XDS. *Acta Crystallogr. D Biol. Crystallogr.* **66**, 125–132 (2010).
63. Vagin, A. & Teplyakov, A. Molecular replacement with MOLREP. *Acta Crystallogr. D Biol. Crystallogr.* **66**, 22–25 (2010).
64. Murshudov, G. N. et al. REFMAC5 for the refinement of macromolecular crystal structures. *Acta Crystallogr. D Biol. Crystallogr.* **67**, 355–367 (2011).
65. Zeldin, O. B., Gerstel, M. & Garman, E. F. RADDOSE-3D: time- and space-resolved modelling of dose in macromolecular crystallography. *J. Appl. Crystallogr.* **46**, 1225–1230 (2013).

Acknowledgements

A.L. was funded by a Marie Curie Individual Fellowship within the Horizon 2020 Research and Innovation Framework Programme (748758). The Danish Ministry of Higher Education and Science through the Instrument Center DANSCATT funded travel to synchrotrons. We would also like to acknowledge MAX-IV, Lund, Sweden, the ESRF, Grenoble, France and DESY, Hamburg, Germany for synchrotron beamtime and related assistance. We thank J.-C. Poulsen for technical assistance; A. Kohler and D. Thiele for helpful discussions; F. Chaspoul for assistance with ICP-MS analyses

and R. Balestrini (Institute for Sustainable Plant Protection, Italy) for providing gold-labeled WGA lectin. L.L.L. and T.T. thank the Novo Nordisk Foundation for funding through grant NF17SA0027704. K.E.H.F. thanks the Carlsberg Foundation through an Internationalization Postdoc Fellowship (grants CF16-0673 and CF17-0533) and the EU, framework of the Marie Curie FP7 COFUND People Programme (AgreenSkills+ fellowship 609398) for financial support. L.L.L., T.T. and K.E.H.F. are members of ISBUC Integrative Structural Biology at the University of Copenhagen (https://isbuc.ku.dk/). K.S.J. thanks the Novo Nordisk Foundation for funding through grant NNF17SA0027704. P.H.W. and L.C. thank the UK Biotechnology and Biological Sciences Research Council (BB/L021633/1) for funding. F.M. is funded by the French National Research Agency through the Laboratory of Excellence Advanced Research on the Biology of Tree and Forest Ecosystems (grant ANR-11-LABX 0002 01). A.Z. thanks the French Embassy in Greece, together with the French Ministry of Higher Education, Research and Innovation, for the scholarship 'Séjour scientifique de haut niveau' (SSHN). The electron microscopy experiments were performed on the PiCSL-FBI core facility (IBDM, Marseille), member of the France-BioImaging national research infrastructure (ANR-10-INBS-04).

Author contributions

A.L., D.N. and M.-N.R. identified the new proteins. A.L. and B.H. performed bioinformatic analyses. A.L., S.G. and M.H. performed recombinant protein production and purification. T.T. and K.E.H.F. crystallized LaX325, determined and analyzed the X-ray crystal structure. T.T. collected X-ray data. K.E.H.F. made relevant figures and tables. L.L.L. directed the crystallographic studies. K.E.H.F., K.S.J. and L.L.L. analyzed the structure. K.E.H.F. and L.L.L. drafted relevant parts of the manuscript. A.L., B.B. and A.Z. performed enzyme assays. M.F. and D.R. performed mass spectrometry analyses. L.C. and P.H.W. conceived and carried out the EPR study. A.L. and F.Z. performed confocal microscopy under the supervision of F.M. A.L. and N.B. performed transmission electron microscopy. J.-G.B. coordinated the work. A.L. and J.-G.B. organized the data and drafted the manuscript. All authors made comments on the manuscript and approved the final version.

Competing interests

The authors declare no competing interests.

Additional information

Supplementary information is available for this paper at https://doi.org/10.1038/s41589-019-0438-8.

Correspondence and requests for materials should be addressed to J.-G.B.

Reprints and permissions information is available at www.nature.com/reprints.

nature research

Corresponding author(s): Jean-Guy Berrin

Last updated by author(s): Oct 14, 2019

Reporting Summary

Nature Research wishes to improve the reproducibility of the work that we publish. This form provides structure for consistency and transparency in reporting. For further information on Nature Research policies, see Authors & Referees and the Editorial Policy Checklist.

Statistics

For all statistical analyses, confirm that the following items are present in the figure legend, table legend, main text, or Methods section.

n/a	Confirmed	
☐	☒	The exact sample size (*n*) for each experimental group/condition, given as a discrete number and unit of measurement
☐	☒	A statement on whether measurements were taken from distinct samples or whether the same sample was measured repeatedly
☒	☐	The statistical test(s) used AND whether they are one- or two-sided *Only common tests should be described solely by name; describe more complex techniques in the Methods section.*
☒	☐	A description of all covariates tested
☒	☐	A description of any assumptions or corrections, such as tests of normality and adjustment for multiple comparisons
☒	☐	A full description of the statistical parameters including central tendency (e.g. means) or other basic estimates (e.g. regression coefficient) AND variation (e.g. standard deviation) or associated estimates of uncertainty (e.g. confidence intervals)
☒	☐	For null hypothesis testing, the test statistic (e.g. *F*, *t*, *r*) with confidence intervals, effect sizes, degrees of freedom and *P* value noted *Give P values as exact values whenever suitable.*
☒	☐	For Bayesian analysis, information on the choice of priors and Markov chain Monte Carlo settings
☒	☐	For hierarchical and complex designs, identification of the appropriate level for tests and full reporting of outcomes
☒	☐	Estimates of effect sizes (e.g. Cohen's *d*, Pearson's *r*), indicating how they were calculated

Our web collection on statistics for biologists contains articles on many of the points above.

Software and code

Policy information about availability of computer code

Data collection	Plasmalab softaware -Thermo-Electron) was used to determine copper concentration
Data analysis	Muscle was used for multiple sequence alignment; Fasttree (v2.1) was used to infer phylogenies for alignments and Booster to complete phylogenetic analysis.

For manuscripts utilizing custom algorithms or software that are central to the research but not yet described in published literature, software must be made available to editors/reviewers. We strongly encourage code deposition in a community repository (e.g. GitHub). See the Nature Research guidelines for submitting code & software for further information.

Data

Policy information about availability of data

All manuscripts must include a data availability statement. This statement should provide the following information, where applicable:

- Accession codes, unique identifiers, or web links for publicly available datasets
- A list of figures that have associated raw data
- A description of any restrictions on data availability

LaX325 nucleotide sequence was deposited in GenBank under accession number MK088083. The X-ray structures of LaX325 were deposited in the Protein Data Bank with accession numbers 6IBH, 6IBI, 6IBJ. Raw EPR data are available on request through the Research Data York (10.15124/a034974e-2782-415e-8b02-2b6e4098760e).

Field-specific reporting

Please select the one below that is the best fit for your research. If you are not sure, read the appropriate sections before making your selection.

☒ Life sciences ☐ Behavioural & social sciences ☐ Ecological, evolutionary & environmental sciences

For a reference copy of the document with all sections, see nature.com/documents/nr-reporting-summary-flat.pdf

Life sciences study design

All studies must disclose on these points even when the disclosure is negative.

Sample size	No methods were used to determine sample size. We believe that sample size is sufficient for the present study. Usually, triplicate measurements are performed for characterization of enzymes.
Data exclusions	No data were excluded.
Replication	All attempts at replication were successful. Different protein batches were produced and gave similar results.
Randomization	No randomized methods were used. These methods are not relevant to the characterization of enzymes.
Blinding	Most of the experiments were done to look for enzymatic activity of X325 proteins and therefore we believe that blinding was not relevant to this study.

Reporting for specific materials, systems and methods

We require information from authors about some types of materials, experimental systems and methods used in many studies. Here, indicate whether each material, system or method listed is relevant to your study. If you are not sure if a list item applies to your research, read the appropriate section before selecting a response.

Materials & experimental systems

n/a	Involved in the study
☐	☒ Antibodies
☒	☐ Eukaryotic cell lines
☒	☐ Palaeontology
☒	☐ Animals and other organisms
☒	☐ Human research participants
☒	☐ Clinical data

Methods

n/a	Involved in the study
☒	☐ ChIP-seq
☒	☐ Flow cytometry
☒	☐ MRI-based neuroimaging

Antibodies

Antibodies used	An anti-LbX325 antibody was raised in rabbit in the frame of this study (supplier Eurogentec). It was used with a dilution 1/20. The donkey-anti-rabbit 6nm gold-labelled IgG was from (Aurion). The dilution was 1/15. The 15 nm gold-labelled lectin (WGA) that binds to fungal chitin was provided by Raffaella Balestrini (Italy).
Validation	The rabbit anti-LbX325 antibody was validated using L. bicolor S238N crude extracts (see Suppl. Figure 6).